Photocatalytic water splitting with acridine dyes: Guidelines from computational chemistry

Xiaojun Liu [a,b], Tolga N.V. Karsili [a], Andrzej L. Sobolewski [c], Wolfgang Domcke [a,*]

[a] Department of Chemistry, Technical University of Munich, D-85747 Garching, Germany
[b] Key Laboratory of Luminescence and Optical Information, Ministry of Education, Institute of Optoelectronic Technology, Beijing Jiaotong University, Beijing 100044, PR China
[c] Institute of Physics, Polish Academy of Sciences, PL-02668 Warsaw, Poland

ABSTRACT

The photocatalytic splitting of water into H· and OH· radicals in hydrogen-bonded chromophore-water complexes has been explored with computational methods for the chromophores acridine orange (AO) and benzacridine (BA). These dyes are strong absorbers within the range of the solar spectrum. It is shown that low-lying charge-transfer excited states exist in the hydrogen-bonded AO—H_2O and BA—H_2O complexes which drive the transfer of a proton from water to the chromophore, which results in AOH·—OH· or BAH·—OH· biradicals. The AOH· and BAH· radicals possess bright $\pi\pi^*$ excited states with vertical excitation energies near 3.0 eV which are predissociated by a low-lying repulsive $\pi\sigma^*$ state. The conical intersections of the $\pi\sigma^*$ state with the $\pi\pi^*$ excited states and the ground state provide a mechanism for the photodetachment of the H-atom by a second photon. Our results indicate that AO and BA are promising chromophores for water splitting with visible light.

© 2015 The Authors. Published by Elsevier B.V. This is an open access article under the CC BY license (http://creativecommons.org/licenses/by/4.0/).

1. Introduction

Splitting of water into H· and OH· radicals *via* photosensitization with a redox-active chromophore which absorbs within the range of the solar spectrum could be a particularly straightforward and cost-efficient way of generating clean and sustainable energy directly from sunlight. The ideal catalyzer for this reaction should absorb strongly in the visible and be able to abstract a hydrogen atom from a water molecule in its excited state. Denoting the photocatalyzer by X, the first step of the water-splitting reaction is:

$$X - H_2O + h\nu \rightarrow X^* - H_2O \qquad (1)$$

$$X^* - H_2O \rightarrow \quad XH\cdot + OH\cdot, \qquad (2)$$

where X—H_2O denotes a hydrogen-bonded complex of the chromophore X with a water molecule. By photodetachment of the surplus H-atom from the XH· radical with a second photon

$$XH\cdot + h\nu \rightarrow X + H\cdot, \qquad (3)$$

the photocatalyzer X is recovered and a water molecule has been split into H· and OH· radicals. Exothermic radical–radical recombination reactions may yield H_2 and H_2O_2 as closed-shell products. H_2O_2 can finally be catalytically decomposed into H_2O and O_2.

In recent work, we explored the mechanisms of the photoreactivity of pyridine (Py) and acridine (Ac) in hydrogen-bonded complexes of Py and Ac with a single water molecule using state-of-the-art computational methods [1–3]. We constructed minimum-energy reaction paths, their energy profiles and two-dimensional relaxed potential-energy (PE) surfaces for H-atom transfer from water to Py and Ac, respectively, in low-lying $\pi\pi^*$ and $n\pi^*$ excited states in the singlet and triplet manifolds. The results reveal the mechanisms by which photoexcited Py or Ac can abstract an H-atom from water *via* an electron-driven proton-transfer process. A key finding were hitherto unknown excited states of charge-transfer character (involving electron promotion from the p-orbital of water to the π^* orbital of the chromophore) which are separated by low energy barriers from the spectroscopic states of the chromophore-water complexes. The charge-separated electronic states are strongly lowered in energy by the transfer of a proton from water to the chromophore, which results in XH·—OH· (X = Py, Ac) biradicals. The excess energy of the H-atom transfer reaction is sufficient to dissociate the biradicals into X· and OH· free radicals. Due to the existence of a low-lying repulsive $^2\pi\sigma^*$ state in the XH· radicals, the radicals can be photodissociated with a second photon. This regenerates the Py or Ac chromophores, which thus become photocatalyzers [1–3].

While Py absorbs in the far UV, Ac absorbs at 450 nm in aqueous solution [4] and thus at the upper edge of the solar spectrum at the surface of earth. Therefore, both chromophores are not suitable

---

* Corresponding author.
  E-mail address: domcke@ch.tum.de (W. Domcke).

catalyzers for efficient water splitting with sunlight. Herein, we explore the photochemistry of two chromophores derived from acridine which absorb well within the solar spectrum, acridine orange (tetramethylacridine-3,6-diamine) (AO) and benzacridine (BA). The aim of this work is to provide evidence that these easily accessible chromophores are potential photocatalyzers for the splitting of water with sunlight. Ab initio multi-configuration multi-reference perturbation methods as well as propagator methods were employed for the calculation of electronic excitation energies, excited-state reaction paths and conical intersections among the relevant electronic states of the AO—H_2O and BA—H_2O complexes as well as of the AOH· and BAH· radicals.

In earlier investigations of the Py—H_2O and Ac—H_2O complexes, we explored the reaction mechanisms in both singlet and triplet manifolds [1–3]. While the bright $^1\pi\pi^*$ electronic states are populated by the absorption of light, the triplet states may come into play by intersystem crossing (ISC), which may compete with direct photoreactions in the singlet manifold. It was found that the topographies of the PE surfaces of the triplet states are quite similar to those of the singlet states in Py—H_2O and Ac—H_2O (see Refs. [1–3] for details). Since the excited-state electronic-structure calculations are considerably more tedious and expensive for the larger chromophores considered herein, we have confined the calculations to the singlet manifold.

2. Computational methods

The second-order Møller–Plesset (MP2) method was employed for the determination of the ground-state equilibrium geometries of the AO—H_2O and BA—H_2O complexes. Vertical excitation energies were calculated with the complete-active-space self-consistent-field (CASSCF) method, the CASPT2 method (second-order perturbation theory with respect to the CASSCF reference) as well as with the ADC(2) method. ADC(2) is a single-reference many-body Green's function method [5,6]. Vertical excitation energies, geometries of minimum-energy reaction paths and saddle points on the excited-state PE surfaces were determined with the ADC (2) method. Although ADC(2) is a single-reference method, it has been found to be reliable for the prediction of vertical excitation energies of singly-excited states of closed-shell systems [7]. In particular, ADC(2) PE surfaces are well behaved near conical intersections of exited electronic states, although the method may possibly fail near conical intersections of excited states with the electronic ground state. In recent investigations of the pyridine-water complex, we evaluated the accuracy of the ADC(2) method in comparison with CASSCF/CASPT2 results [1,2]. It was shown that the ADC (2) method is a qualitatively reliable and computationally efficient alternative to multi-reference perturbation methods and coupled-cluster-type methods for the calculation of excitation energies and the characterization of local regions of excited-state PE surfaces for such systems. Therefore, most of the calculations in the present work, in particular all excited-state geometry optimizations, were performed with the ADC(2) method. Being derived by diagrammatic perturbation theory for systems with a closed-shell ground state, ADC(2) is not readily applicable to the open-shell AOH· and BAH· radicals. The calculations for the AOH· and BAH· radicals were therefore performed with the CASSCF and CASPT2 methods.

The reaction paths were constructed as so-called relaxed scans. For the calculation of the reaction path for the H-atom-transfer process from water to the N-atom of the chromophore, the bond length of the OH bond of the water molecule involved in hydrogen bonding was chosen as the driving coordinate, while all other internal nuclear coordinates of the complex were relaxed in the electronic state under consideration. The distance between the O-atom of H_2O and the N-atom of the chromophore was taken as the second driving coordinate in the calculation of

two-dimensional PE surfaces in the vicinity of the saddle point of the H-transfer reaction. The latter calculations were performed as rigid scans on a two-dimensional grid in the R_{OH} and R_{ON} coordinates, since two-dimensional relaxed scans turned out to be prohibitively time-consuming. The reaction path for the photodetachment of the hydrogen atom from the AOH· and BAH· radicals was constructed as a rigid scan of the NH bond length, because the relaxation of the internal coordinates of the system is of little importance in this case [8]. The saddle points for the H-atom transfer reactions were estimated from the two-dimensional relaxed PE surfaces. The minimum-energy geometries of conical intersections were optimized using the CIOpt program of Martinez and coworkers [9].

In the CASSCF calculations for the chromophore-H_2O complex, 14 electrons were distributed in 13 orbitals, including the five highest π and five lowest π^* orbitals the chromophore, the n orbital of the N-atom, one p orbital of the O-atom and the lowest σ^* orbital of water. The energies of the S_0 state and the lowest $^1\pi\pi^*$ and $^1n\pi^*$ states were averaged with equal weights in the calculations of the singlet states. The active space of the CASSCF calculations for the XH· radicals (X = AO, BA) consisted of 13 electrons in 12 orbitals: the five highest π orbitals and five lowest π^* orbitals of the chromophore as well as one σ orbital and one σ^* orbital of the NH bond. The CASPT2 calculations for the vertical excitation energies were carried out as single-state, single-reference calculations and a level shift of 0.3 au was employed. For the calculation of the PE functions for hydrogen detachment, a smaller active space had to be employed due to the computational cost of these calculations and due to convergence problems with the larger active space. This smaller active space consisted of 10 electrons in 9 orbitals: the four highest π orbitals and three lowest π^* orbitals of the chromophore as well as one σ orbital and one σ^* orbital of the NH bond. The state-averaging included the three lowest A' and the three lowest A'' states.

The MP2 and ADC(2) calculations were carried out with the TURBOMOLE program package [10], making use of the resolution-of-the-identity (RI) approximation [11]. The CASSCF and CASPT2 calculations were performed with the MOLPRO program package [12]. C_s symmetry (that is, co-planarity of the water molecule with the chromophore) was enforced throughout the calculations. The correlation-consistent split-valence double-ζ basis set with polarization functions on all atoms (cc-pVDZ) [13] was employed in the calculations for the AO—H_2O and BA—H_2O complexes. The Rydberg character of the $^2\sigma^*$ state of the AOH· and BAH· radicals requires the augmentation of the cc-pVDZ basis with diffuse basis functions. The aug-cc-pVDZ basis was therefore employed for the calculation of the PE functions of the D_0, $^2\pi\pi^*$ and $^2\pi\sigma^*$ states of the radicals.

3. Results

3.1. Equilibrium geometries and vertical excitation energies of the AO—H_2O and BA—H_2O complexes

The equilibrium structures of the AO—H_2O and BA—H_2O complexes, optimized at the MP2 level with C_s symmetry constraint, are shown in Fig. 1. The H_2O molecule acts as a hydrogen bond donor to the N-atom acceptor of the chromophore. The vertical excitation energies of the three lowest singlet states (two $^1\pi\pi^*$ states and one $^1n\pi^*$ state) calculated with the CASSCF, CASPT2 and ADC(2) methods are given in Table 1. The vertical excitation energies of the Ac—H_2O complex are shown for comparison (slight deviations of the CASPT2 excitation energies of Ac—H_2O from those reported in Ref. [3] are due to differences in the state averaging of the CASSCF reference wave function).
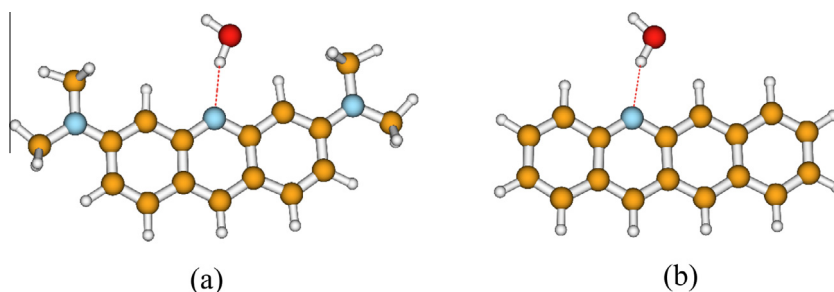
Fig. 1. Equilibrium geometry of the electronic ground state of the AO—H$_2$O (a) and BA—H$_2$O (b) hydrogen-bonded complex calculated with C_s symmetry constraint.

Table 1
Vertical excitation energies (in eV) and the oscillator strengths (in parentheses) of the AO—H$_2$O and BA—H$_2$O hydrogen-bonded complexes. The data for Ac—H$_2$O [3] are included for comparison.

	Ac—H$_2$O			AO—H$_2$O			BA—H$_2$O		
	$^1\pi\pi^*$	$^1\pi\pi^*$	$^1n\pi^*$	$^1\pi\pi^*$	$^1\pi\pi^*$	$^1n\pi^*$	$^1\pi\pi^*$	$^1\pi\pi^*$	$^1n\pi^*$
ADC (2)	3.70 (0.092)	3.90 (0.050)	4.12 (0.001)	2.91 (0.085)	3.11 (0.349)	4.08 (0.001)	2.81 (0.079)	3.50 (0.053)	3.80 (0.001)
CASSCF	4.02 (0.024)	4.72 (0.081)	5.03 (0.005)	3.77 (0.192)	4.35 (0.034)	6.00 (0.005)	3.81 (0.094)	4.03 (0.039)	4.77 (0.005)
CASPT2	3.33	3.71	4.28	2.94	3.22	4.43	2.75	2.98	3.99

For all three complexes, the two $^1\pi\pi^*$ states are the lowest excited singlet states. For AO—H$_2$O and BA—H$_2$O, the energy of the lowest singlet excited state is lower than the lowest singlet state of Ac—H$_2$O by about 0.8 eV at the ADC(2) level. At the CASPT2 level, the lowering of the energies of the $^1\pi\pi^*$ states of AO—H$_2$O and BA—H$_2$O relative to Ac—H$_2$O is less pronounced (about 0.5 eV), which may be a consequence of the limitation of the active space to 13 orbitals, which is more restrictive for the larger π-systems. The $^1n\pi^*$ state is substantially higher in energy than the two lowest $^1\pi\pi^*$ states (it is blue-shifted relative to the isolated chromophore). Since it does not carry oscillator strength, it will not be considered in what follows. The oscillator strengths of the $^1\pi\pi^*$ states are about the same for the three chromophores (at the ADC(2) level, which is considered to be more reliable for response properties).

### 3.2. PE surfaces for excited-state H-atom transfer from water to the chromophore

Fig. 2 shows energy profiles along minimum-energy reaction paths for H-atom transfer from the hydrogen-bonded water molecule to the chromophore. The energy profiles were constructed as relaxed scans at the ADC(2) level. The reaction coordinate R_{OH} is the bond length of the OH group involved in the hydrogen-bonding between the H$_2$O molecule and the N-atom of the chromophore. Small values of R_{OH} ($\approx$1.0 Å) correspond to the equilibrium geometry of the chromophore-H$_2$O complex. Large values of R_{OH} ($\approx$2.5 Å) correspond to a biradical structure, consisting of the hydrogenated chromophore and the OH$\cdot$ radical. The vertical dashed line in Fig. 2a–c separates the reaction path optimized in the electronic ground state (black dots for R_{OH} < 1.2 Å) from the reaction path optimized in the lowest charge-transfer (CT) state (red squares for R_{OH} > 1.2 Å). The energies of the remaining states were computed along these optimized reaction paths.

The PE profiles to the left of the vertical dashed line show the ordering of the excited states in the Franck–Condon (FC) region. The PE functions of these locally excited states are seen to be parallel to the ground-state PE function. These states are thus non-reactive with respect to the transfer of a proton or H-atom from the solvent molecule to the chromophore. The pronounced lowering of the energy of the lowest $^1\pi\pi^*$ state in AO—H$_2$O and BA—H$_2$O

relative to the lowest $^1\pi\pi^*$ state of Ac—H$_2$O is clearly visible. The PE functions to the right of the dashed vertical line, designated as $^1\pi\pi^*$(CT) and $^1n\pi^*$(CT), on the other hand, correspond to CT states in which an electron has been transferred from a p-orbital of H$_2$O to the lowest π^* orbital (LUMO) of the chromophore. It is seen that the energies of the CT states are strongly stabilized by the transfer of a proton from H$_2$O to the chromophore. This electron-driven proton-transfer (EDPT) process [8] results in electronic states of biradical character. The energy of the closed-shell electronic ground state, on the other hand, moves up in energy by several electron volts in all three systems upon the transfer of a proton. The energy of the ground state crosses the energy of the optimized $^1\pi\pi^*$(CT) state at R_{OH} = 1.50 Å, 1.65 Å and 1.43 Å, respectively, in Ac—H$_2$O, AO—H$_2$O and BA—H$_2$O. The crossing of the S_0 energy with the $^1n\pi^*$ energy is allowed by symmetry, while the crossing of the S_0 energy with the $^1\pi\pi^*$ energy is a weakly avoided crossing. These energy crossings become conical intersections when out-of-plane vibrational modes are taken into account. The $^1\pi\pi^*/S_0$ and $^1n\pi^*/S_0$ conical intersections coalesce, in fact, into a $^1\pi\pi^*/^1n\pi^*/S_0$ three-state conical intersection. We located the minimum energy of this three-state intersection at the CASSCF level without symmetry constraints. The location of the optimized three-state conical intersection with respect to energy and R_{OH} is marked by the green star in Fig. 2a–c.
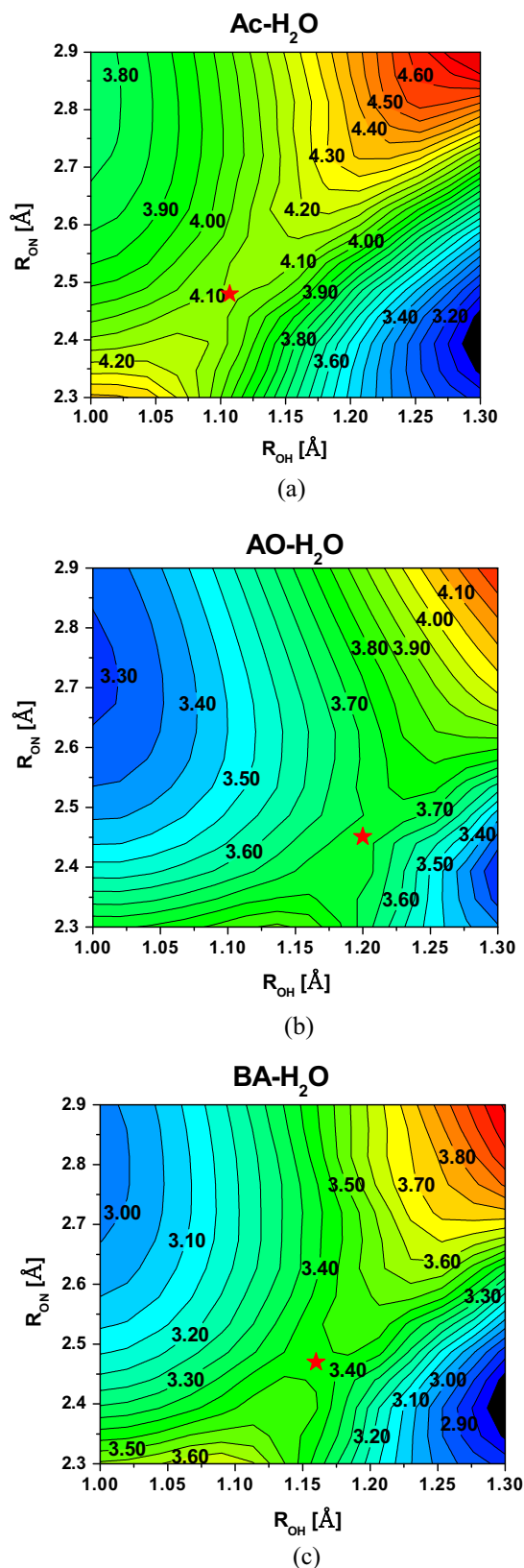
At the $^1\pi\pi^*/S_0$ and $^1n\pi^*/S_0$ conical intersections, nonadiabatic transitions from the CT excited states to the S_0 state can take place. If these transitions happen, the H-bonded complex is restored in its electronic and vibrational ground state after vibrational energy relaxation on the S_0 surface. Otherwise, $^1\pi\pi^*$ or $^1n\pi^*$ biradicals are formed. The excess energy available from the proton transfer reaction is by far sufficient to break the weak hydrogen bond between the radicals, resulting in free XH$\cdot$ and OH$\cdot$ radicals (X = Ac, AO, BA).

Inspection of Fig. 2 reveals that the locally excited (spectroscopic) $^1\pi\pi^*$ states as well as the CT $^1\pi\pi^*$ states are lowered in energy by the extension of the π-conjugated system. This bathochromic shift in the electronic absorption is attributable to a larger density of π and π^* orbitals upon increasing conjugation. As a result, the barrier (relative to the minimum of the locally excited $^1\pi\pi^*$ state) which connects the locally excited (LE) and the charge-separated singlet states near R_{OH} = 1.2 Å, is approximately

(a)

(b)

(c)
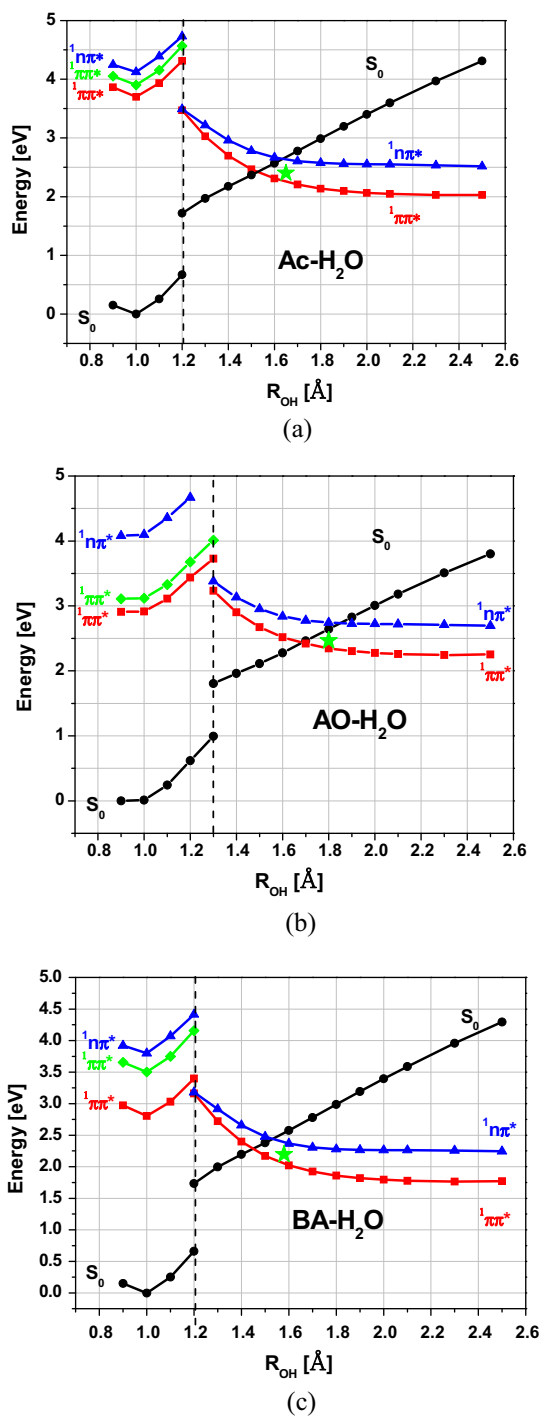
Fig. 2. Energy profiles of minimum-energy reaction paths for excited-state hydrogen transfer from water to Ac, (a) AO (b) and BA, (c) calculated with the ADC (2) method. The reaction coordinate is the bond length R_{OH} of the OH group of water involved in hydrogen bonding with the N-atom of the chromophore. The energy profiles to the left of the vertical dashed line were calculated for the reaction path optimized in the electronic ground state (black dots). The energy profiles to the right of the vertical dashed line were calculated for a reaction path which was optimized in the lowest $\pi\pi^*$(CT) state (red squares). The energies of the remaining states were calculated at the geometries of these optimized reaction paths. (For interpretation of the references to color in this figure legend, the reader is referred to the web version of this article.)

(a)

(b)

(c)

Fig. 3. PE surface of the lowest $^1\pi\pi^*$ excited state in the vicinity of the barrier for H-atom transfer from water to the chromophore, calculated with the ADC(2) method for Ac—H$_2$O, (a) AO—H$_2$O (b) and BA—H$_2$O. (c) The reaction coordinates are the OH bond length R_{OH} of water and the distance R_{ON} from the oxygen atom of water to the nitrogen atom of the chromophore. The red star indicates the estimated saddle point. (For interpretation of the references to color in this figure legend, the reader is referred to the web version of this article.)

the same for the three chromophores. To visualize these barriers explicitly, rigid scans of the PE surfaces as functions of the R_{OH} and R_{ON} (the distance between the oxygen atom of H$_2$O and the

N-atom of the chromophore) were computed with the ADC(2) method and are displayed in Fig. 3. These two-dimensional energy surfaces display the adiabatic connection of the $\pi\pi^*$ PE curve (red) on the left hand side of Fig. 2 to the $\pi\pi^*$ PE curve (red) on the right hand side of Fig. 2. For Ac—H_2O, the rigid scan shown in Fig. 3a can be compared with the corresponding relaxed scan shown in Fig. 5b of Ref. [3]. Although the energy of the peak of the barrier with respect to the S_0 minimum is about 0.2 eV higher in the rigid scan than in the relaxed scan, the barrier height with respect to the $^1\pi\pi^*$(LE) minimum is the same ($\approx$0.4 eV). This result indicates that the barriers relevant for H-atom transfer in chromophore-water complexes can be reliably estimated from rigid scans. Fig. 3b and c reveal that the barrier height for H-atom tunneling relative to the $^1\pi\pi^*$(LE) minimum is about 0.5 eV in both AO—H_2O and BA—H_2O and thus marginally higher than in Ac—H_2O. The somewhat larger barrier height suggests that the rate of H-atom tunneling from the water molecule to the chromophore may be lower in the AO—H_2O and BA—H_2O complexes than in the Ac—H_2O complex.

3.3. Vertical excitation energies and PE functions for H-atom photodetachment from the radicals

The lowest vertical excitation energies of the AcH·, AOH· and BAH· radicals, calculated with the CASPT2 method, are given in Table 2. The lowest excited state is of $^2\pi\pi^*$ character and corresponds to the excitation from the highest doubly occupied π orbital (HOMO) to the singly occupied π orbital (SOMO). The next two $^2\pi\pi^*$ states correspond to excitation from HOMO and HOMO-1 to the lowest unoccupied π orbital (LUMO). The $^2\pi\sigma^*$ state corresponds to the excitation from the HOMO to the σ^* orbital, which is antibonding with respect to the NH bond. At the ground-state equilibrium geometry, the σ^* orbital is of 3s Rydberg character and localized outside the π-conjugated system, which renders the $^2\pi\sigma^*$ state highly polar. Upon extension of the NH bond, the σ^* orbital collapses to the 1s orbital of the H-atom, as is well known for pyrrole, indole and related systems [14]. As shown by Table 2, the vertical excitation energy of the $^2\pi\sigma^*$ state is lowest in AOH· and highest in BAH·. In AcH· and BAH·, the vertical $^2\pi\sigma^*$ excitation energy is above all three $^2\pi\pi^*$ excited states. In AOH·, on the other hand, the $^2\pi\sigma^*$ state is quasi-degenerate with the second $^2\pi\pi^*$ state. The $^2\pi\sigma^*$ state is dark, while the three $^2\pi\pi^*$ states carry comparable oscillator strengths.

Although the $^2\pi\sigma^*$ state cannot be excited directly by light, it can be populated by vibronic coupling with quasi-degenerate $^2\pi\pi^*$ states or via a radiationless transition from the higher-lying $^2\pi\pi^*$ states. The mechanisms of the H-atom photodetachment reaction from the AcH·, AOH· and BAH· radicals are illustrated by the NH-stretching PE profiles displayed in Fig. 4. While the PE functions of the three $^2\pi\pi^*$ excited states are bound with respect to the NH-stretching coordinate, the PE function of the $^2\pi\sigma^*$ state is, apart from a low barrier, strongly repulsive. The $^2\pi\sigma^*$ PE function crosses the PE functions of the $^2\pi\pi^*$ states as well as that of the electronic ground state (D_0). These crossings are symmetry-allowed crossings, since the ground state and the $^2\pi\pi^*$ states transform as A″ in C_s symmetry, while the $^2\pi\sigma^*$ state transforms as A′.

The energy crossings become conical intersections when out-of-plane vibrational coordinates are taken into account. The repulsive $^2\pi\sigma^*$ state opens a channel for efficient H-atom photodetachment from the radicals. It should be noted that the dissociation threshold of the $^2\pi\sigma^*$ state of AOH·, at 2.5 eV, is less than half of the dissociation threshold of the ground state. In BAH·, the dissociation threshold of the $^2\pi\sigma^*$ state is about 0.5 eV higher. When the $^2\pi\pi^*$ states are excited below the minimum of the crossing seam with the $^2\pi\sigma^*$ state, H-atom photodetachment can occur by tunneling, as is well established for phenol, for example [15–17]. When the $^2\pi\pi^*$ states are excited above the minimum of the $^2\pi\pi^*$/$^2\pi\sigma^*$ crossing seam, a rapid nonadiabatic transition to the $^2\pi\sigma^*$ state is expected to take place, followed by ultrafast dissociation through the $^2\pi\sigma^*$/D_0 conical intersection or, alternatively, internal conversion to the D_0 state of the radical. For closed-shell systems like pyrrole and phenol, the efficient predissociation of the bound $^1\pi\pi^*$ states by repulsive $^1\pi\sigma^*$ states has been experimentally confirmed [18–20]. In the AcH·, AOH· and BAH· radicals, one or two additional bound $^2\pi\pi^*$ PE surfaces have to be crossed by the dissociating wave packet on the $^2\pi\sigma^*$ PE surface. The effect of these additional surface crossings on the quantum yield of H-atom detachment should be explored by future quantum dynamics calculations.

4. Discussion and conclusions

Ab initio electronic-structure calculations were employed in this work to explore the photochemistry of the AO—H_2O and BA—H_2O hydrogen-bonded complexes. We have characterized the minimum-energy reaction paths connecting the locally excited singlet states of the chromophores to hitherto unknown charge-separated excited states. These CT states are difficult to find in the FC region of the complexes because they are high in energy, are strongly mixed with the spectroscopic $^1\pi\pi^*$ and $^1n\pi^*$ states and their energies are very sensitive to the geometry of the complex. However, the CT states become the lowest electronic states of the AO—H_2O or BA—H_2O complexes when a proton moves from the H_2O molecule to the chromophore, as shown in Fig. 2. When the proton is fully transferred, the electronic charge separation is neutralized. The reaction products are XH·—OH· (X = AO, BA) neutral biradicals. The excess energy available after the EDPT process is sufficient to dissociate the biradicals, which yields XH· and OH· free radicals. A substantial part of the energy of the photon is stored as chemical energy in these radicals.

The topographies of the $^1\pi\pi^*$ and $^1n\pi^*$ PE surfaces in the vicinity of the barrier for proton transfer from H_2O to the chromophore were characterized by two-dimensional scans as functions of the R_{OH} and R_{ON} coordinates at the ADC(2) level. Barriers of the order of 0.5 eV relative to the minimum of the lowest locally excited $^1\pi\pi^*$ state were determined, which indicates hydrogen atom transfer from water to the chromophore may occur by tunneling on time scales of hundreds of picoseconds to nanoseconds. The results obtained for the AO—H_2O and BA—H_2O complexes were compared with earlier results obtained for the Ac—H_2O complex with the same computational methods [3]. As expected, the first two spectroscopic $^1\pi\pi^*$ states of AO and BA are significantly lower in energy than in Ac due to the extension of the π-conjugation. Importantly,

Table 2

Vertical excitation energies (in eV) and the oscillator strengths (in parentheses) of the AOH· and BAH· radicals. The data for the AcH· radical [3] are included for comparison.

	AcH·				AOH·				BAH·			
	$^2\pi\sigma^*$	$1^2\pi\pi^*$	$2^2\pi\pi^*$	$3^2\pi\pi^*$	$^2\pi\sigma^*$	$1^2\pi\pi^*$	$2^2\pi\pi^*$	$3^2\pi\pi^*$	$^2\pi\sigma^*$	$1^2\pi\pi^*$	$2^2\pi\pi^*$	$3^2\pi\pi^*$
CASSCF	2.54	2.79	3.50	3.61	2.09	3.07	3.33	3.56	2.76	2.67	3.03	3.46
	(0.000)	(0.005)	(0.040)	(0.043)	(0.000)	(0.015)	(0.020)	(0.008)	(0.000)	(0.007)	(0.014)	(0.017)
CASPT2	2.96	2.12	2.48	2.65	2.45	2.10	2.42	2.63	3.16	2.09	2.28	2.61

it has been found in the present work that the energies of the CT states are lowered by roughly the same amount as the energies of the spectroscopic states. Consequently, the barrier separating the locally-excited $^1\pi\pi^*$ states and the charge-separated $^1\pi\pi^*$ states is approximately the same in all three systems.

ISC may compete with the singlet-state driven photochemistry of organic chromophores. For Py—H$_2$O and Ac—H$_2$O, the topographies of the $^3\pi\pi^*$ and $^3n\pi^*$ states were explored in earlier work [1–3]. The topographies of the PE surfaces of the triplet states were found to be largely similar to those of the singlet states. The lowest locally excited $^3\pi\pi^*$ state is special in so far as it is much lower in energy than the lowest $^1\pi\pi^*$ state in the FC region due to the large exchange matrix element in extended organic systems. As a result, the barrier connecting the lowest spectroscopic $^3\pi\pi^*$ state with the lowest $^3\pi\pi^*$(CT) state is substantial (≈ 0.8 eV in Ac—H$_2$O [3]) and most likely even higher in AO—H$_2$O and BA—H$_2$O). The existence of a long-lived $^3\pi\pi^*$ state in these complexes indicates the possibility of a two-photon excitation process, wherein the first photon excites one of the low-lying $^1\pi\pi^*$ states. After ISC and internal conversion within the triplet manifold to the long-lived lowest $^3\pi\pi^*$ state, a triplet–triplet absorption may take the system to a higher triplet state [21,22], from which a barrierless H-atom-transfer reaction can readily take place. While more input of excitation energy is required, it is likely that the photoreactions are barrierless and that the quantum yields of the relevant processes are high *via* this mechanism.

The second step of the water-splitting reaction is the photodetachment of the surplus H-atom from the AOH· or BAH· radicals. Our calculations reveal that these hypervalent aromatic radicals exhibit low-lying (≈ 3.0 eV) bound $^2\pi\pi^*$ PE functions which are intersected by dissociative $^2\pi\sigma^*$ PE functions. The repulsive $^2\pi\sigma^*$ state intersecting the two light-absorbing $^2\pi\pi^*$ states and the ground state provides a channel for H-atom photodetachment. While the $^1\pi\sigma^*$ driven photodetachment of closed-shell aromatic chromophores with acidic groups is nowadays experimentally well established and theoretically well understood [15–20], such photoreactions have hitherto received much less experimental and theoretical attention for radicals. The conical intersections of the lowest $^2\pi\sigma^*$ state with several bound $^2\pi\pi^*$ states in the radicals may cause a trapping of the population of the $^2\pi\sigma^*$ state *en route* to dissociation, which may reduce the overall yield of H· photoproducts, depending on the strength of the nonadiabatic couplings at the $^2\pi\sigma^*$/$^2\pi\pi^*$ conical intersections. This issue deserves further investigation by quantum dynamics calculations based on accurate ab initio PE surfaces.

Fig. 5 gives an overview of the theoretically estimated absorption spectra of Ac—H$_2$O, AO—H$_2$O and BA—H$_2$O and the corresponding AcH·, AOH· and BAH· radicals in comparison with the solar spectrum at the surface of earth. An empirical bandwidth of 0.3 eV FWHM was chosen for the simulated spectra. While Ac is seen to absorb at the upper edge of the solar spectrum, the absorption profiles of AO and BA fully overlap with the high-energy part of the solar spectrum, see Fig. 5a. Further extension of the π-conjugated system, e.g. in dibenzacridine, will lead to a further bathochromic shift of the absorption profile. Fig. 5b shows that the absorption profiles of the AcH·, AOH· and BAH· radicals exhibit good overlap with the high-energy part of the solar spectrum. It is suggested that AO and BA are promising lead structures for the development of simple and efficient organic water-oxidation photocatalysts.

The available experimental data indicate that Ac and AO can photo-abstract hydrogen atoms from hydrocarbons and alcohols, although not from water [23–25]. However, the photo-oxidation potential of the chromophores can be manipulated by suitable substitution. Electron-withdrawing substituents, such as cyano
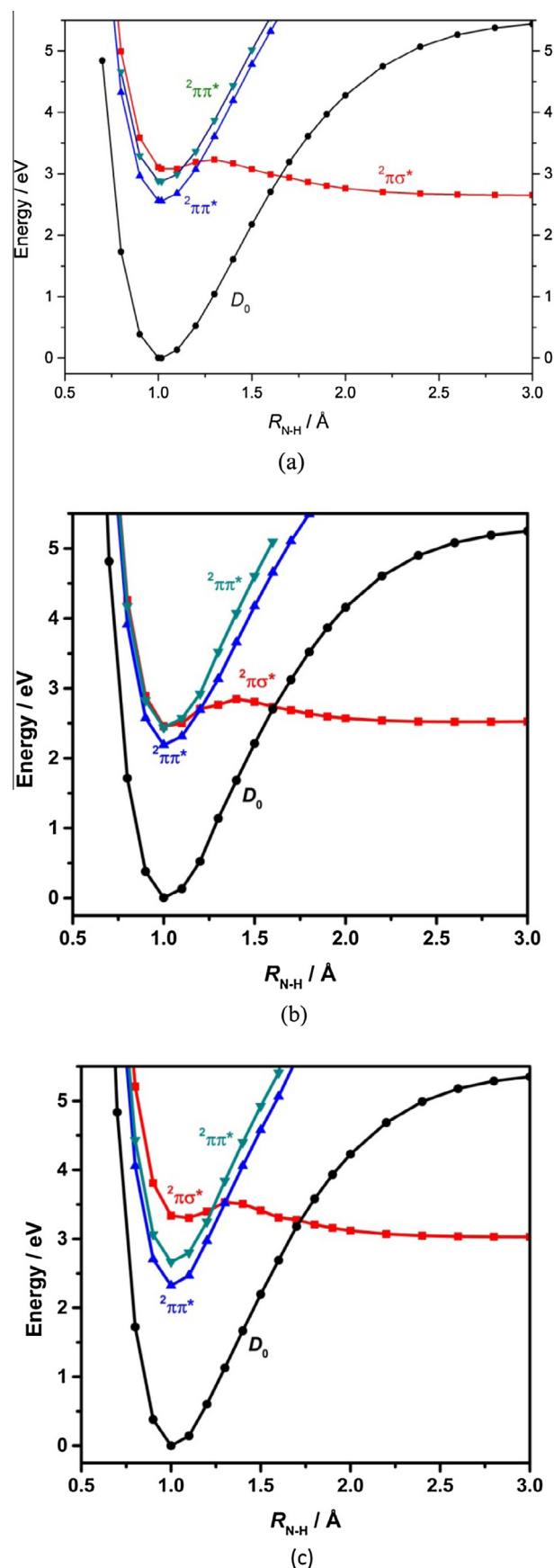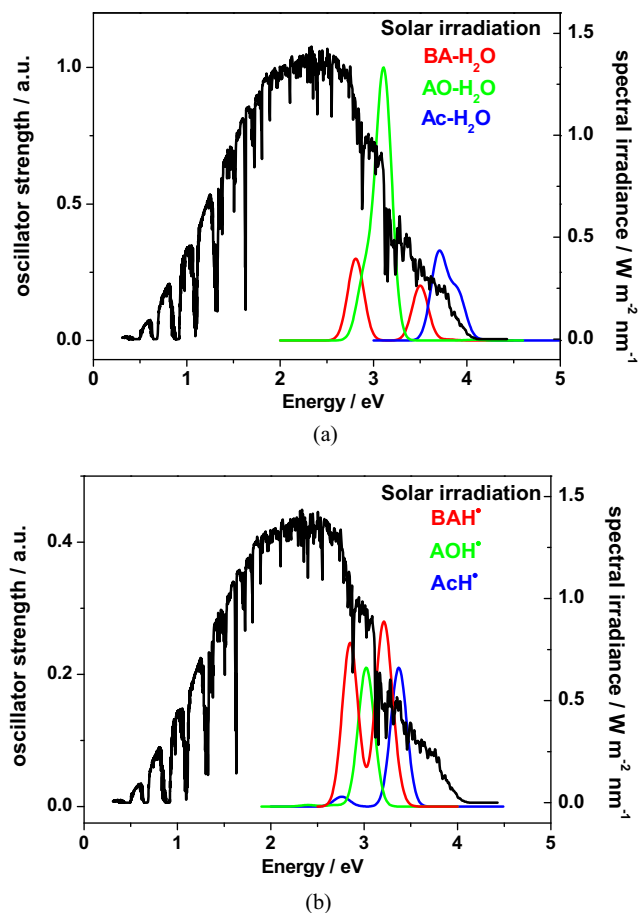

Fig. 4. Energy profiles for the photodetachment reaction of the hydrogen atom from the AcH·, (a) AOH· (b) and BAH· (c) radicals, calculated at the CASPT2 level.

Fig. 5. (a) Absorption spectra of Ac—H$_2$O (blue), AO—H$_2$O (green) and BA—H$_2$O (red) in comparison with the solar spectrum at the surface of earth (black). (b) Absorption spectra of the AcH$^\cdot$ (blue), AOH$^\cdot$ (green) and BAH$^\cdot$ (red) radicals in comparison with the solar spectrum at the surface of earth (black). (For interpretation of the references to color in this figure legend, the reader is referred to the web version of this article.)

groups, may lower the energy of the CT states in the X—H$_2$O complexes and may consequently lower the barriers for H-atom transfer from the solvent to the chromophore. We postulate on the basis of the present computational results that suitably substituted AO or BA chromophores should be able to photo-oxidize neat water with measurable yields. The hydroxyl radicals can be scavenged and detected by their reaction with benzoic acid, salicylic acid or terephtalic acid. The hydroxylated forms of these non-fluorescent acids are strongly fluorescent and the build-up of the characteristic fluorescence is proportional to the formation rate of the OH$^\bullet$ radicals [26].

Alternatively to H-atom photodetachment from the intermediate radicals, the latter may serve as reducing agents. Evidence has been reported in recent years that the pyridinyl radical (PyH$^\cdot$) is an exceptionally strong reducing agent which can even reduce CO$_2$ to formaldehyde, formic acid or methanol with suitable catalyzers [27–29], albeit the mechanisms of these reactions are currently poorly understood [30–32]. The theoretically predicted dissociation thresholds of the AcH$^\cdot$, AOH$^\cdot$ and BAH$^\cdot$ radicals are about 2.7 eV, 2.5 eV and 3.0 eV, respectively (see Fig. 4), while the predicted dissociation threshold of the pyridinyl radical is much lower, about 1.7 eV [1]. Pyridinyl is thus a significantly stronger reductant than acridinyl and related radicals. It is therefore not expected that the latter will be able to reduce carbon dioxide in dark reactions.

Another issue of considerably practical interest in photoinduced water splitting is chemical damage of the photocatalyzer by the highly reactive OH$^\cdot$ radicals generated in the water-splitting reaction. Since OH$^\cdot$ radicals primarily attack aromatic systems by abstracting hydrogen atoms from CH groups, perhalogenation may considerably enhance the robustness of the aromatic chromophores. In addition, OH$^\cdot$ radical scavengers such as benzoic acid or manganese oxide may be employed to suppress undesired hydroxylation reactions in future exploratory water-splitting experiments.

Very recently, Eisenhart and Dempsey demonstrated the formation of AOH$^\cdot$ radicals by excitation of a solution of 40 μM AO and 1 mM tri-tert-butylphenol in acetonitrile at 425 nm [33]. The authors tracked intermediates with nanosecond time-resolved spectroscopy and demonstrated the efficient formation of AOH$^\cdot$ radicals by photoinduced coupled electron/proton transfer from phenol to AO. Phenol is somewhat easier to oxidize than water and thus can serve as a sacrificial agent for photoinduced water splitting. A 100 μs lifetime was established for the AOH$^\cdot$ radial under these conditions [33]. This lifetime should be sufficient to demonstrate the photodetachment of the H-atom from the AOH$^\cdot$ radical with photons of about 500 nm, as proposed in the present work. In aqueous or alcoholic solutions, the photoejected H-atoms form solvated electrons with appreciable quantum yield [34–36]. The latter can conveniently be detected by their strong and characteristic absorption near 750 nm [37].

Conflict of interest

The authors declare that there is no conflict of interest.

Acknowledgments

References

[1] X. Liu, A.L. Sobolewski, R. Borelli, W. Domcke, Phys. Chem. Chem. Phys. 15 (2013) 5957.
[2] X. Liu, A.L. Sobolewski, W. Domcke, J. Phys. Chem. A 118 (2014) 7788.
[3] X. Liu, T.N.V. Karsili, A.L. Sobolewski, W. Domcke, J. Phys. Chem. B 119 (2015) 10664.
[4] E.T. Ryan, T. Xiang, K.P. Johnston, M.A. Fox, J. Phys. Chem. A 101 (1997) 1827.
[5] J. Schirmer, Phys. Rev. A 26 (1982) 2395.
[6] A.B. Trofimov, J. Schirmer, J. Phys. B: At. Mol. Opt. Phys. 28 (1995) 2299.
[7] M. Wormit, D.R. Rehn, P.H.P. Harbach, J. Wenzel, C.M. Krauter, E. Epifanovski, A. Dreuw, Mol. Phys. 112 (2014) 774.
[8] A.L. Sobolewski, W. Domcke, J. Phys. Chem. A 111 (2007) 11725.
[9] B.G. Levine, J.D. Coe, T.J. Martinez, J. Phys. Chem. A 112 (2008) 405.
[10] R. Ahlrichs, M. Bär, M. Häser, H. Horn, C. Kölmel, Chem. Phys. Lett. 162 (1989) 165.
[11] C. Hättig, F. Weigend, J. Chem. Phys. 113 (2000) 5154.
[12] H.-J. Werner, P. Knowles, G. Knizia, F.R. Manby, M. Schütz, P. Celani, T. Korona, R. Lindh, A. Mitrushenkov, G. Rauhut, MOLPRO 2006.1, A Package of Ab Initio Programs, University College Cardiff Cons. Lt., Cardiff, Wales, 2006.
[13] T.H. Dunning Jr., J. Chem. Phys. 90 (1989) 1007.
[14] A.L. Sobolewski, W. Domcke, C. Dedonder-Lardeux, C. Jouvet, Phys. Chem. Chem. Phys. 4 (2002) 1093.
[15] R.N. Dixon, T.A.A. Oliver, M.N.R. Ashfold, J. Chem. Phys. 134 (2011) 194303.
[16] G.M. Roberts, A.S. Chatterley, J.D. Young, V.G. Stavros, J. Phys. Chem. Lett. 3 (2012) 348.
[17] Z. Lan, W. Domcke, V. Vallet, A.L. Sobolewski, S. Mahapatra, J. Chem. Phys. 122 (2005) 224315.
[18] M.N.R. Ashfold, B. Cronin, A.L. Devine, R.N. Dixon, M.G.D. Nix, Science 312 (2006) 1637.

[19] M.N.R. Ashfold, G.A. King, D. Murdock, M.G.D. Nix, T.A.A. Oliver, A.G. Sage, Phys. Chem. Chem. Phys. 12 (2010) 1218.
[20] G.M. Roberts, V.G. Stavros, Chem. Sci. 5 (2014) 1698.
[21] Y. Hirata, T. Tanaka, Chem. Phys. 25 (1977) 381.
[22] N. Periasamy, Chem. Phys. Lett. 99 (1983) 322.
[23] D.G. Whitten, Y.J. Lee, J. Am. Chem. Soc. 93 (1971) 961.
[24] K. Kasama, K. Kikuchi, S. Yamamoto, U. Koji, Y. Nishida, H. Kokubun, J. Phys. Chem. 85 (1981) 1291.
[25] K. Kikuchi, K. Kasama, A. Kanemoto, U. Koji, H. Kokubun, J. Phys. Chem. 89 (1985) 868.
[26] O. Morawski, K. Izdebska, E. Karpiuk, J. Nowacki, A. Suchocki, A.L. Sobolewski, Phys. Chem. Chem. Phys. 16 (2014) 15256.
[27] E.B. Cole, P.S. Lakkaraju, D.M. Rampulla, A.J. Morris, E. Abelev, A.B. Bocarsly, J. Am. Chem. Soc. 132 (2010) 11539.
[28] Y. Yan, E.L. Zeitler, J. Gu, Y. Hu, A.B. Bocarsly, J. Am. Chem. Soc. 135 (2013) 14020.
[29] F. Riboni, E. Selli, M.R. Hoffmann, A.J. Colussi, J. Phys. Chem. A 119 (2015) 4433.
[30] J.A. Keith, E.A. Carter, J. Am. Chem. Soc. 134 (2012) 7580.
[31] C.H. Lim, A.M. Holder, C.B. Musgrave, J. Am. Chem. Soc. 135 (2013) 142.
[32] M.Z. Ertem, S.J. Konezny, C.M. Araujo, V.S. Batista, J. Phys. Chem. Lett. 4 (2013) 745.
[33] T.T. Eisenhart, J.L. Dempsey, J. Am. Chem. Soc. 136 (2014) 12221.
[34] D.V. Bent, E. Hayon, J. Am. Chem. Soc. 97 (1975) 2599.
[35] D.V. Bent, E. Hayon, J. Am. Chem. Soc. 97 (1975) 2612.
[36] A.L. Sobolewski, W. Domcke, J. Phys. Chem. A 105 (2001) 9275.
[37] F.Y. Chou, G.R. Freeman, J. Phys. Chem. 83 (1979) 5570.